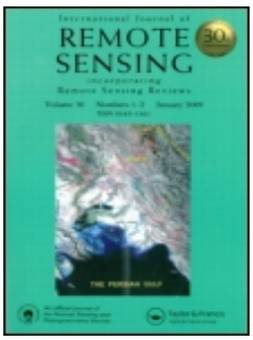

International Journal of Remote Sensing

ISSN: 0143-1161 (Print) 1366-5901 (Online) Journal homepage: https://www.tandfonline.com/loi/tres20

Generating soil electrical conductivity maps at regional level by integrating measurements on the ground and remote sensing data

P. Brunner , H. T. Li , W. Kinzelbach & W. P. Li

To cite this article: P. Brunner , H. T. Li , W. Kinzelbach & W. P. Li (2007) Generating soil electrical conductivity maps at regional level by integrating measurements on the ground and remote sensing data, International Journal of Remote Sensing, 28:15, 3341-3361, DOI: 10.1080/01431160600928641

To link to this article: https://doi.org/10.1080/01431160600928641

Published online: 31 Jul 2007.

International Journal of Remote Sensing
Vol. 28, No. 15, 10 August 2007, 3341–3361

Taylor & Francis
Taylor & Francis Group

Generating soil electrical conductivity maps at regional level by integrating measurements on the ground and remote sensing data

P. BRUNNER*†, H. T. LI‡, W. KINZELBACH† and W. P. LI‡

†Institute of Environmental Engineering (IfU), ETH, Zurich 8093, Switzerland
‡China Institute of Geoenvironmental Monitoring, 20 Dahuisi, Haidian District, Beijing 100081, People's Republic of China

(*Received 6 April 2006; in final form 13 June 2006*)

In arid and semi-arid areas, salinization of soil and water resources is one of the major threats to irrigated agriculture. For management purposes, quantifying both the extent and distribution of salinization is important, but accurate data with sufficient spatial resolution are often not available. Commonly used techniques such as soil sampling and geophysical methods are time-consuming and yield only point data. A method is described in which multispectral remote sensing images can be used to regionalize point data measured on the field. Field data consist of measurements of electrical conductivity and are obtained by the combination of geophysical methods and the analysis of field soil samples. Uncalibrated salinity maps were calculated with spectral correlation mapping using image-based reference spectra of saline areas. As an alternative indicator for soil salinity, the NDVI was used. The method was verified in the Yanqi Basin, northwestern China. Correlations between field data and the uncalibrated salinity maps were found over non-irrigated sites for all images. Good correlations (R^2 up to 0.85) resulted for images collected during the winter months. The high correlation coefficients allow the uncalibrated salinity maps to be scaled to electrical conductivity maps.

1. Introduction

Salinization occurs naturally (primary salinization) or due to human activities (secondary salinization). Comprehensive overviews covering most of its causes and consequences as well as ways to tackle the problem can be found in Hillel (2000) and Jakeman *et al.* (1995), just to mention a few examples. According to Oldeman *et al.* (1991), 76.6 Mha of farmland, which amounts to about 30% of the global irrigated area, is in one way or the other affected by human-induced salinization. The consequences of soil salinity have accompanied societies that rely on irrigated agriculture through history. Various historical and current examples are described by Hillel (1990).

Considering the severe economic and ecological consequences of soil salinization, quantifying its distribution and extent is crucial for the management of affected areas. A recent review article (Metternicht and Zinck 2003) discusses several salinity mapping methods and their possible constraints. As a possible processing procedure for the raw remote sensing data, Metternicht and Zinck mention the optimum index factor (Dwivedi and Rao 1992), image transformations such as the principle

*Corresponding author. Email: brunner@ifu.baug.ethz.ch

International Journal of Remote Sensing
ISSN 0143-1161 print/ISSN 1366-5901 online
http://www.tandf.co.uk/journals
DOI: 10.1080/01431160600928641

component analysis and band ratios such as the NDVI (Wiegand *et al.* 1994), intensity hue saturation transformations and unmixing of surface features. Moreover, a fuzzy classification based on JERS-1 SAR data has been described. Including information such as geomorphic positions or different soil types into the spectral analysis may improve the results, as shown by Metternicht and Zinck (1997). Besides the processing procedures, several image data sources for mapping soil salinity are discussed: various airborne and spaceborne sensors can be used, including sensors covering the visible to middle infrared (Csillag *et al.* 1993, Rao *et al.* 1995, Kalra and Joshi, 1996), thermal infrared (Mulders, 1987) and microwave sensors (Singh *et al.* 1990, Taylor *et al.* 1996). Airborne hyperspectral data are listed as one of the most promising sources of data to discriminate between different kinds of salt and soils. Examples of the use of hyperspectral imagery can be found in the literature (Ben-Dor *et al.* 2002, Taylor, 2000, Howari, 2003b, Howari *et al.* 2002).

Despite all the potential factors that limit the precise and direct estimation of salt quantities from satellite remote sensing, Metternicht and Zinck conclude that good monitoring results can be obtained by integrating remote sensing data with field and laboratory data. In this paper, a new method is described which allows soil salinity to be mapped in terms of electrical conductivity over large areas. This method, in full agreement with the final conclusion of Metternicht and Zinck, consists of a combination of field data and uncalibrated salinity maps calculated from spaceborne multispectral images. The field data consist of measurements of electrical conductivity. They were obtained by the combination of geophysical methods and the measurement of the saturated paste conductivities of soil samples.

2. Site description

The Yanqi Basin is located in the far west of China (see figure 1). The climate is continental and very dry. The annual amount of rain of around 20 mm/year is

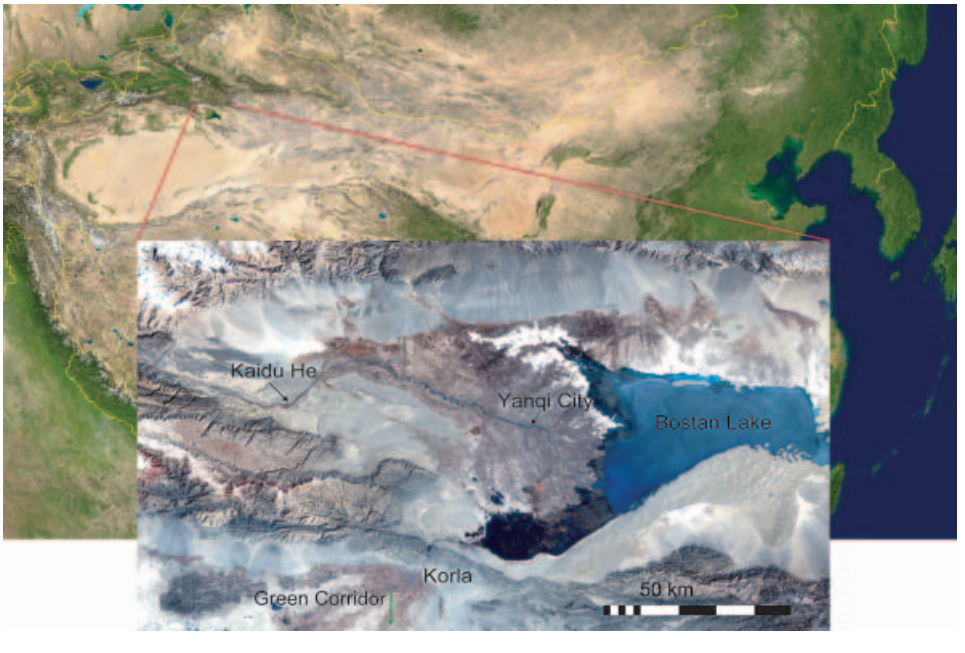

Figure 1. Location of the Yanqi Basin.

negligible compared with the potential evapotranspiration (ET) of 1200 mm/year (data for year 2000). Precipitation is far too small to remove accumulating salt from the soil. Nevertheless, the Yanqi Basin has been one of the most productive agricultural areas in western China ever since irrigation channels were constructed in the second half of the twentieth century. At present, the irrigated area covers about 1.2×10^5 ha. A large amount of water is wasted owing to ineffective supply systems and inefficient farm irrigation practices. The main water source is the Kaidu River. The Kaidu River flows through the Basin into Bostan Lake. The Kaidu River also recharges the underlying aquifer. Except for areas in the immediate vicinity of the lake shore, the pre-irrigation groundwater table was >5 m below the surface. In 2000, 60% of the entire irrigation area exhibited a groundwater table of <2 m below the surface (Dong *et al.* 2001). This rise in the groundwater table triggered the salinity problem.

Water resources in the Yanqi Basin are sufficient, therefore agriculture can be kept at a very high level by periodically leaching salts into the aquifer. As a consequence, the productivity of the downstream systems is strongly affected by the non-sustainable water and salt management in the Yanqi Basin.

3. Methods and data acquisition

3.1 *Overview*

The study consists of three major parts: (1) obtaining field data in terms of electrical conductivity of the soil (see §3.2); (2) calculating uncalibrated salinity maps (see §3.3); and (3) combining these two data sets (see §4).

The three major steps required to calculate electrical conductivity maps are characterized by different spatial scales. Field data are obtained at point scale (single electrical conductivity measurements) and transformed to a pixel scale by averaging several measurements. The second step is on the scale of raster maps from satellite images. It consists of calculating uncalibrated salinity maps. Combining this raster map with field data on a pixel scale is the final step. A diagram illustrating these different scales and their combination is shown in figure 2. The single steps are discussed in detail in the following sections.

3.2 *Field data*

A wide range of methods exists to measure electrical conductivity of soils. Summaries covering most of these procedures can be found in Rhoades *et al.* (1999). Several standardized procedures have been suggested to measure soil salinity from soil samples: a selection of different methods to analyze soil samples was presented by Richards (1954). Besides the classical procedures of analysing soil samples, indirect methods to quantify soil salinity have been developed.

One indirect method is based on Faraday's law. A transmitter coil induces circular eddy loops in the soil. Each loop induces a secondary electromagnetic field; a fraction of the secondary field is intercepted by the receiver coil, producing a voltage output. This voltage is directly proportional to a depth-weighted electrical conductivity. A wide range of instruments based on the induction law has been developed. Details about the principle and a description of some sensors are discussed in McNeill (1992).

Another, classical method to indirectly quantify electrical conductivity of the soil is resistivity soundings (geoelectrics). A current is fed into the soil via current

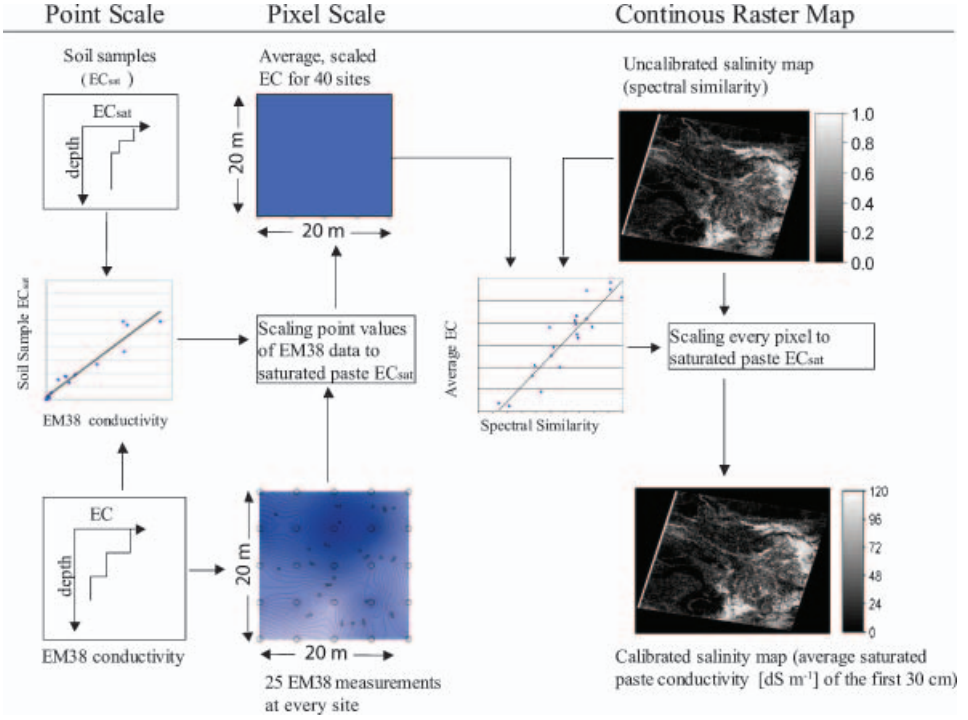

Figure 2. Overview of the major steps and scales.

electrodes. The induced potential is measured with two other electrodes, called potential electrodes. A one-dimensional electrical conductivity profile can be obtained by inverting the relationship between the electrode spacing and the measured resistivity (Telford *et al.* 1990, Rhoades and Miyamoto 1990).

All methods have their specific advantages and limitations. One common constraint of resistivity and induction methods is the requirement of a minimal amount of water. Rhoades *et al.* (1992) stated that measurements on soils with less than 10% water per weight are not a reliable indicator of the extent of salinity.

Although taking soil samples is expensive and time-consuming, a measure of electrical conductivity independent of the field conditions can be determined. Moreover, data such as the water content, the amount of salt in the sample and the chemical composition of the salts present can be determined.

Electromagnetic induction using the EM38 (manufactured by Geonics) allows to quickly map the extent of soil salinity to a depth of around 2 meters. An EM38 measurement is performed within seconds by one single person. Although a measure for electrical conductivity can be obtained quickly, the EM38 measurements must be interpreted to obtain an electrical conductivity profile. The big advantage of resistivity measurements is that they are not restricted to a certain depth. The effective depth of exploration is about one-third of the distance between the current electrodes (Halvorson and Rhoades 1976). In contrast to EM38 measurements, resistivity soundings can take over an hour and are best performed by several people.

All three methods were used in combination. Only the EM38 allows large areas to be mapped within a reasonable time. Soil samples, on the other hand, yield absolute

values of electrical conductivity. It is therefore straightforward to combine these two methods: if EM38 data can be correlated with electrical conductivity data obtained through the analysis of soil samples, the relation found can be used to scale the interpreted EM38 data. To quantify electrical conductivity values in the areas with a large depth to groundwater, four-pole resistivity measurements in the Schlumberger array were performed.

3.2.1 Measurement sites and layout. Field data were obtained in two field campaigns in the Yanqi Basin (September to October 2002 and September 2003). In the first campaign, measurements were mainly performed over non-irrigated sites. The second campaign consisted of some additional Schlumberger measurements along the northern boundaries, as well several EM38 measurements over irrigated areas. It was not possible to perform all three methods at every station. For example, EM38 measurements do not make sense along the northern boundaries of the Basin as the depth of interest is much larger than the exploration depth of the EM38. Therefore, only Schlumberger soundings were performed in these areas. Figure 3 summarizes the locations of the stations and indicates what kind of measurements were carried out.

At 17 sites, soil samples were taken and Schlumberger soundings as well as EM38 measurements were performed. At six locations, only EM38 measurements were carried out and soil samples were taken. Seven locations were documented by Schlumberger measurements as well as EM38 measurements (in figure 3, these seven points are not distinguished explicitly from the Schlumberger sites). At 21 locations, only EM38 measurements were carried out. At three sites, only soil samples were taken (not plotted in figure 3).

All the measurements applied yield one-dimensional vertical profiles of electrical conductivity at a point. With regard to the goal, to correlate measurements on the ground with remote sensing data, point values are not sufficient. A pixel recorded by a multi-spectral sensor represents the spectral properties of the combination of the materials present over the whole pixel area. Salts tend to accumulate in patches. Point measurements of electrical conductivity therefore may not be representative for the average electrical conductivity covered by one pixel of the satellite. It is

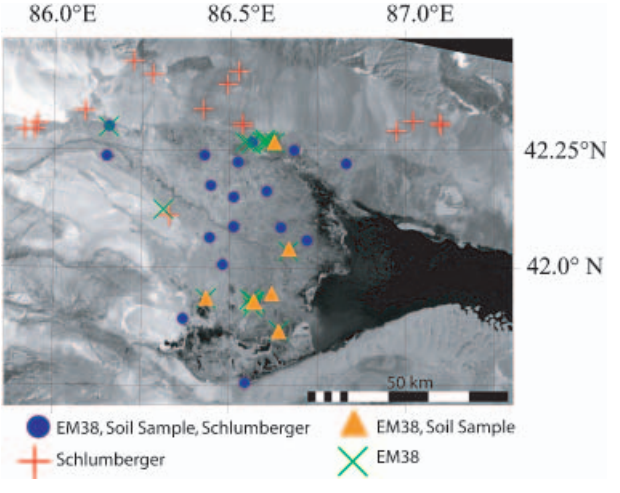

Figure 3. Measurement sites in the Yanqi Basin.

therefore necessary to perform several measurements over an area with a spatial extent comparable to the resolution of the sensor used and then relate an average of several measurements at specific locations on the ground with the raster data. At every EM38 station, 25 EM38 measurements distributed regularly over a square 20 m × 20 m were performed (see figure 4). This is the spatial resolution of the raster data used.

3.2.2 Soil samples. The most common way to describe electrical conductivity independent of the soil water content is the saturated paste conductivity, discussed and described by several authors, e.g. Rhoades (1996). This approach was used in our study. The soil samples were dried. Distilled water was then added until the soil was saturated. The saturated past is the electrical conductivity of the saturation extract. To correct the influence of temperature, electrical conductivity was scaled to the standard temperature of 25°C. In total, 142 soil samples were taken from different depths at 26 sites. Soil samples were obtained with a hand Auger after the EM38 measurements and Schlumberger soundings were completed. The sampled soil was sealed in PET containers to prevent evaporative loss. The thickness of sub-samples varied from 20 to 35 cm. At five stations, soil samples were obtained every 10 cm.

Besides electrical conductivity, the main chemical components of the saturated paste solution as well as the water content of the samples were determined. Measured saturated paste conductivities covered a range from 0.29 up to 167 dS m^{-1}. The difference between irrigated and non-irrigated locations is very clear. Typical electrical conductivity and soil moisture profiles of a non-irrigated and a recently irrigated site are plotted in figure 5. Electrical conductivity and water content of the non-irrigated station 16 (41°55.642′ N, 86°34.402′ E) show a pronounced evaporative profile built up through the continuous evaporation of groundwater. The depth to groundwater at station 16 is only about 2 m, which explains the very high water contents at this site. The irrigated plot at station 3 (42°15.549′ N, 86°29.989′ E) shows no pronounced profile both in the water content and in electrical conductivity. The amount of water required to saturate the soil

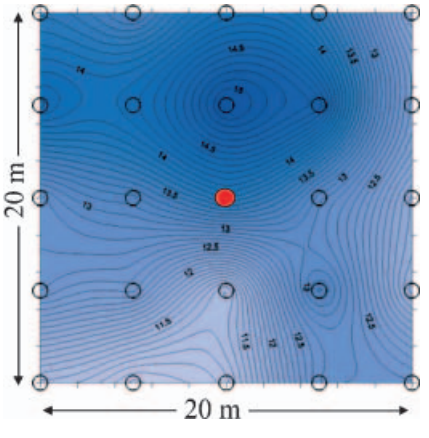

Figure 4. Measurement layout of an EM38 station. It consists of 25 single EM38 measurements (indicated by the circles). If soil samples were taken or a Schlumberger sounding was performed, it was always in the centre of this measurement layout (indicated by the red circle).

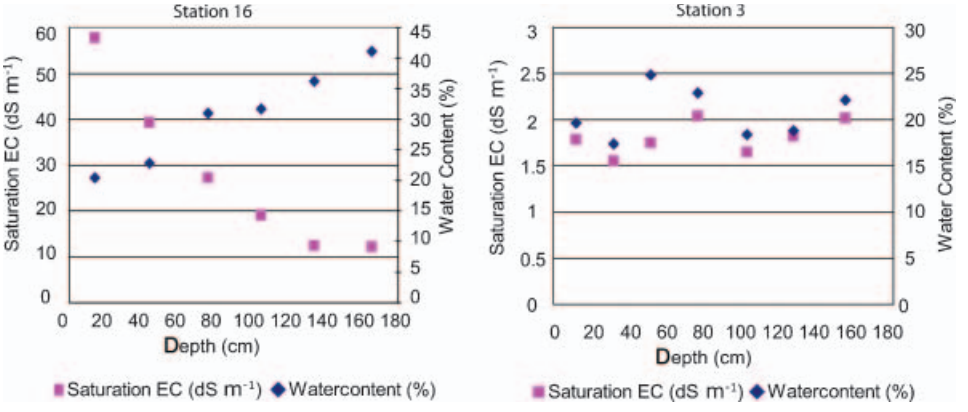

Figure 5. Soil moisture and electrical conductivity profiles for the non-irrigated Station 16 and the irrigated Station 3. The *x*-axis indicates the depth from which the samples were taken.

samples as well as the principal chemical components, is more or less the same for all irrigated and non-irrigated sites.

3.2.3 EM38. Fifty-one locations were mapped with the EM38. If possible, the EM38 sites were chosen within large areas featuring similar conditions around the measurement layout, for example the centers of large fields. A constraint reducing the number of ideal EM38-sites is the high sensitivity of the instrument. It is impossible to measure in areas with electrical noise present, whether it is from power poles or metal objects.

The EM38 can be operated in a horizontal or a vertical mode, depending on the orientation of the coils to the soil surface plane. The effective measurement depths of the instrument in the standard configuration are about 1 m in the horizontal and 2 m in the vertical dipole mode (Rhoades *et al.* 1999). These differences of relative response can be used to determine an electrical conductivity profile (McNeil, 1980).

If the soil water content falls below 10%, the topsoil is too dry and essentially behaves as an insulating layer, strongly affecting the horizontal EM38 reading. In this case, the dry loose soil should be scraped away before positioning the EM38. In the Yanqi Basin, the dried out topsoils of the non-irrigated sites were generally so thin that no significant differences of the EM38 reading could be observed by comparing a measurement with and without the dry layer. The two exceptions, stations 38 and 11, are discussed in section 3.2.5.

The interpretation of the EM38 raw data has been discussed extensively by several authors, e.g. Geonics Limited (2001), Hendrickx *et al.* (2002), McKenzie *et al.* (1997), Rhoades *et al.* (1999). Following Rhoades *et al.* (1999), the raw data of the EM38 can be inverted and yield a three-layered electrical conductivity profile (0–30, 30–60 and 60–90 cm). Rhoades distinguishes between regular, uniform and inverted profiles. If salinity increases with depth, the profile is called regular; profiles in which salinity decreases with depth are called inverted. The structure of the equation to predict soil electrical conductivity is as follows:

$$\ln \mathrm{EC} = a + b \ln \mathrm{EM_h} + c \ln(\mathrm{EM_h} - \mathrm{EM_v})$$

where $\mathrm{EM_h}$ is the EM38 reading in the horizontal and $\mathrm{EM_v}$ is the EM38 reading in

the vertical mode; a, b and c depend on the type of profile as well as the depth of the layer.

McKenzie *et al.* (1997) pointed out that the EM38 readings are not independent of the field conditions. Various potential influences such as soil temperature or clay content are not taken into account in the models described by Rhoades. If such factors are not explicitly considered, the assumption is made that factors other than salinity influencing the reading are homogeneous over the project area. However, the influence of soil moisture is small, although moisture is directly related to the electrical conductivity under field conditions. If soil moisture is increased while the amount of salt in the soil column is held constant, there will be a trade-off between the decreasing salt concentration and the increasing water content. This trade-off keeps the EM38 reading constant over a large range of electrical conductivity.

3.2.4 Resistivity measurements. Thirty-four Schlumberger soundings were carried out. The sites where resistivity measurements were performed are plotted in figure 3. Micro-soundings were carried out at sites with a depth to groundwater smaller than 5 m. A typical sounding consists of several resistivity measurements with an increasing distance between the current electrodes. In principle, any kind of arrangement between potential and current electrodes can be interpreted. However, the interpretation of the results is simpler for some special geometries of the current and potential electrodes. The Schlumberger geometry was used in this project. In this geometry, the current and potential electrodes have a common midpoint but the distances between adjacent electrodes differ. The calculation of the apparent resistivity (ρ) requires the ''cell'' or ''geometric constant'' (k) of the geometric configuration. The derivation of these constants as well as methods to carry out the inversion of the data can be found in geophysical textbooks (e.g. Telford *et al.* 1990, Lowrie 1997). Every electrical conductivity profile has a corresponding (theoretical) relationship between the spacing of the current electrodes and the apparent resistivity. The interpretation of a Schlumberger sounding therefore consists of obtaining a resistivity profile with a corresponding relationship between spacing of the electrodes and apparent resistivity similar to the observed one.

As in any model approach, the observations can be approximated to any desired goodness of fit by increasing the number of free parameters. In case of resistivity inversion, the number of parameters results from the number of layers used to describe the electrical conductivity profile. An over-parameterized model may be tempting, but leads to non-unique results. The goal is therefore to fit the measurements with a limited number of layers. The thickness of the model layers is, in contrast to the layers describing the EM38 readings, not constant. An example of an inversion (station 17) is presented in figure 6. The resulting apparent resistivities are inversely proportional to the electrical conductivity.

The Schlumberger soundings in the areas with a large depth to groundwater (found in the northern areas of the project region) yielded the smallest electrical conductivity values within the entire Basin. In these areas, soil salinity is so small that it cannot be considered as a problem.

3.2.5 Comparison of the different methods. All three methods yield vertical, electrical conductivity profiles of different discretization. To be comparable, the electrical conductivity profiles of all methods must be transformed to the same discretization. The profiles calculated on the basis of EM38 data consist of three different layers with a vertical extent (depth) of 30 cm. The total depth of electrical

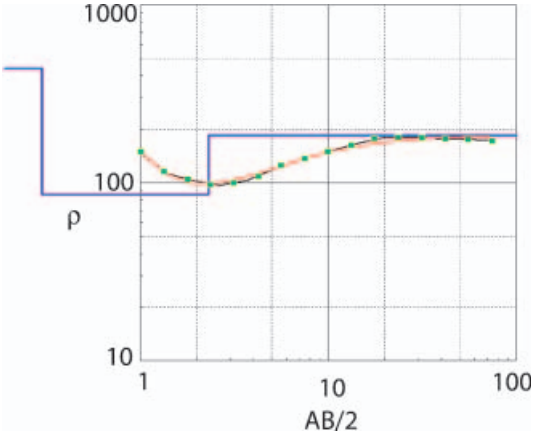

Figure 6. The x-axis (m) represents both the spacing between the source electrodes as well as the depth of modelled resistivity at station 17. Logarithmic resistivity is represented by the y-axis where the red curve indicates the relationship between apparent resistivity ρ; and the spacing between the source electrodes for a soil having a resistivity profile as indicated with the blue curve. The green points are the measured, apparent resistivities at this station.

conductivity profiles obtained from soil samples is not constant. Additionally, the depth of every subsample is not restricted to a constant value.

To compare data obtained with the EM38 to saturated paste conductivities, the saturated paste conductivities were depth-weighted. For all three layers, the conductivities were plotted against each other, see figure 7. The linear regression functions and the corresponding correlation coefficients are presented in table 1. The high correlation coefficients in all layers justify the assumption that factors other than salinity are not influencing the EM38 results significantly. The stations 38 (41°45.379′ N, 86°32.695′ E) and 11 (42°15.02′ N, 86°40.963′ E) are outliers and are not included in the regression. At these stations, salt crusts were present with water contents far below 10%. In contrast to the soil samples, this layer had no influence on the electrical conductivity measured with the EM38. As expected, the saturated paste conductivities are higher than the predicted conductivities obtained with the EM38. The largest discrepancies of the two outliers in the relation found are in the first layer.

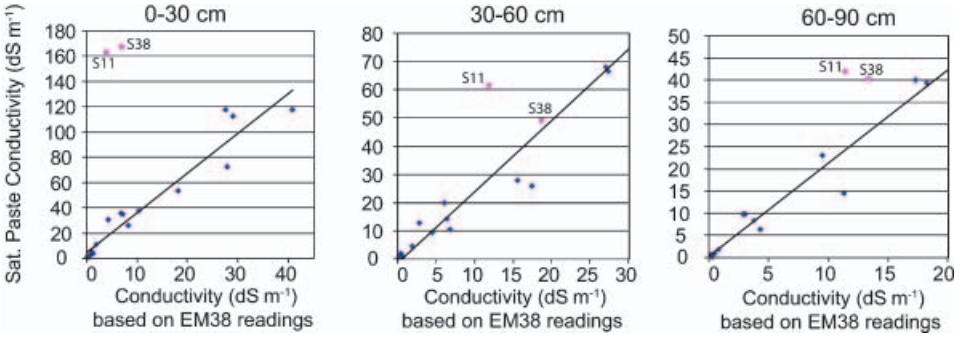

Figure 7. Relationship between saturated paste-conductivities (y-axis, dS m^{-1}) and the EM38 values (x-axis, dS m^{-1}) for the three model layers (left: 0–30 cm, middle: 30–60 cm, right: 60–90 cm). The pink points are outliers.

Table 1. Linear relationships between EM-measurements (x) and saturated paste conductivities of the soil samples (y).

	0–30 cm	30–60 cm	60–90 cm
Function	$y=3.15x+4.5$	$y=2.4x-1.3$	$y=2.25x+0.1$
R^2	0.93	0.96	0.92

Inverted resistivity data were compared in a similar way to the saturated paste conductivities. At every site, the saturated paste conductivities were averaged over a column of the same extent as the model-layers used to describe the resistivity measurements. The comparison between saturated paste conductivities and the reciprocal values of resistivity is plotted in figure 8. The crusts at stations 38 and 11 do not contribute to the Schlumberger measurements; the two stations again are outliers. The difference is not as obvious as with the EM38. The correlation coefficient (obtained without taking the outliers into account) of the linear regression is high ($R^2=0.96$).

Correlations between the methods have been found. Every single EM38 measurement was scaled to saturated paste conductivity. By averaging the 25 EM38 conductivity values at every station, a value on a pixel-scale was obtained (see figures 2 and 4). EM38 measurements at the two outlier stations had to be neglected. Additional soil samples were obtained in order to provide the same spatial information as at all other stations.

3.3 *Remote sensing*

The Terra-Satellite, which carries the ASTER instrument was launched in December 1999. ASTER images of the project region have been available since 2000. The spatial extent of an ASTER image on the ground is approximately 60 by 60 km, not sufficient to map the entire Basin with one image. The ASTER sensor features nine channels covering the spectra from the visible (VNIR) to short-wave (SWIR)

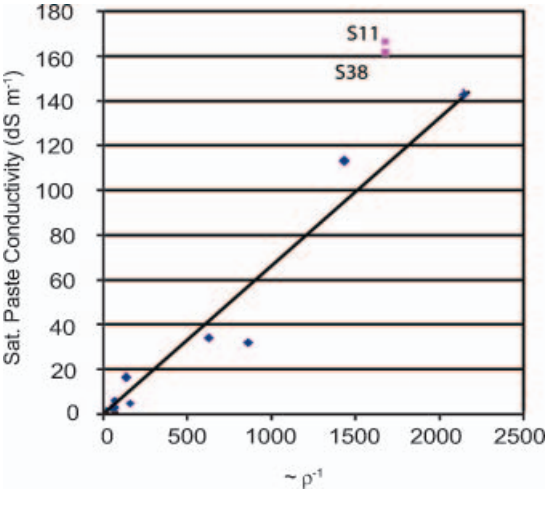

Figure 8. Relationship between saturated paste conductivities (y-axis, dS m^{-1}) and the reciprocal values of the apparent resistivities. The pink points are the outliers (Stations 38 and 11).

infrared with a spatial resolution of 15 and 30 m, respectively. Uncalibrated salinity maps are calculated on the basis of an image-derived reference spectrum. This spectrum consists of the reflectances of the nine channels over one pixel in a extremely saline area. This spectral signature was used to classify every image pixel in terms of spectral similarity. Several algorithms (e.g. Howari 2003a) have been developed to calculate spectral similarity. In this approach a spectral correlation mapper was used (see §3.3.3).

3.3.1 Available remote sensing data and data pre-processing. Data are distributed by the Land Processes Distributed Active Archive Center (LP DAAC), located at the US Geological Survey's EROS Data Center (http://LPDAAC.usgs.gov). The ASTER archive was searched for cloud-free images over the Yanqi Basin. From the beginning of the mission until the end of 2003, 15 images covering the area are available, but only five of them provide a sufficient area coverage as well as cloud-free conditions. The free level2b5 ASTER images were used. These images are atmospherically corrected. The atmospheric correction of the images was performed by the EOS data centre. The detailed description of the algorithms employed and the input data required can be found in Thome (1999). To process the images, the spatial resolution of all channels has to be the same. The spatial resolution applied to calculate salinity maps was 20 m, the same spatial scale as the measurement layout in the field.

Differential GPS data were available for 67 clearly visible surface features in the Yanqi Basin. With this information, the quality of the georeference could be improved, resulting in accuracies in the sub-pixel range.

3.3.2 Image derived reference spectrum. In the approach described in this paper, the reference spectrum was image derived (see figure 9). Although the images were corrected for atmospheric influences, factors such as changes of vegetation or the soil water content influence the spectrum. Differences between spectral responses over the same pixel at different dates are plotted in figure 10. To be consistent, the spectrum used to calculate an uncalibrated salinity map was always obtained from the image processed.

Summer and winter images show a significant difference, not only over the overgrown areas: in wintertime, the spectral responses are much more pronounced. The more pronounced the spectral signatures in different channels are, the clearer different materials can be distinguished. In summertime, the spectral responses over the agricultural area do not show the wide spectral range of the winter images.

The completely salinized station 11 (42°15.02′ N, 86°40.963′ E) was mostly used to derive the reference spectrum. Unfortunately, this station was not contained in all the images processed. If station 11 was not contained in the image processed, other completely salinized locations had to be used instead [e.g. station 38 (41°45.379′ N, 86°32.695′ E)]. Just like station 11, station 38 features a thin salt crust. Both stations have been identified as outliers in figure 7. As the EM38 information could not be used at these specific locations; additional soil samples had to be taken in order to obtain a representative value over an area of the spatial dimension of a pixel.

It is important that the composition of salts at these locations does not differ from other sites. Chemical analysis of the salt crusts at the locations where reference spectra were obtained showed that the salts present and the ratios between their abundances are constant not only for these two stations, but also for other measurement sites (see §3.2.2).

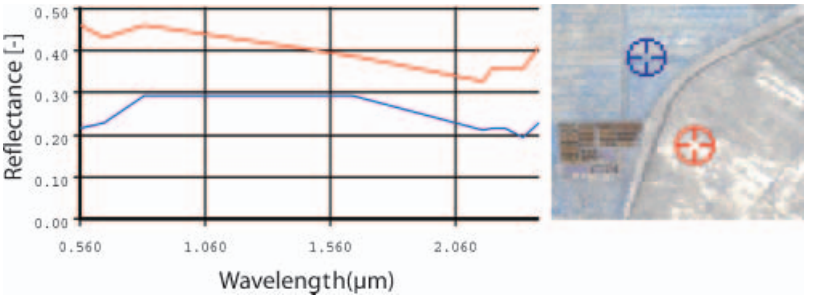

Figure 9. Two examples of an image-derived spectrum from an ASTER image over the project area on 11 November 2002. The reflectance values of two pixels (see left) are plotted as a function of wavelength (see right). The station plotted in red (station 11) could be used as image-derived reference spectrum, as electrical conductivity values observed at this location were very high.

Figure 10. The plot shows the spectral responses of the same, salinized pixel on four different images.

3.3.3 Calculating uncalibrated salinity maps. With the image-derived reference spectrum defined, the spectral similarity of every image pixel to this reference can be calculated. The Spectral Correlation Mapper (SCM) algorithm (de Carvalho and Meneses, 2000) was used to calculate the spectral similarity of every pixel to the image-derived reference spectrum using the software package ERDAS-imagine 8.7. SCM is a modification of the Spectral Angle Mapper (SAM). The SAM (Yuhas *et al.* 1992) derives the angle formed in an *n*-dimensional space between the reference spectrum and the spectrum of every pixel. The dimensionality of space is equal to

the number of channels. The mathematical formula for SAM is the basic vector geometric equation to determine the angle between multidimensional vectors:

$$\alpha = \cos^{-1} \frac{\sum (X \cdot Y)}{\sqrt{\sum (X^2) \cdot \sum (Y^2)}}$$

where α=spectral angle, X=image spectrum and Y=reference spectrum.

This technique is more or less insensitive to changes in pixel illumination, because increasing or decreasing illumination does not change the direction of the vector, only its magnitude. The Spectral Correlation Mapper eliminates this inconsistency by normalizing every vector to the vector mean. For every image processed, the spectral angle of every image pixel to the reference is calculated. Spectral similarity is expressed with the cosine of this angle. Spectral similarity maps were calculated for several dates, both for summer and wintertime.

An example of such an uncalibrated salinity map is shown in figure 11. This image was recorded on 11 November 2002. Irrigated fields are clearly visible: all salt has been leached from the surface, resulting in a very low spectral similarity. Paths or earth walls around the fields are never irrigated, therefore salt can accumulate over time. The value range obtained from spectral similarity stretches from 0 to 1 in this winter image, even within the agricultural area.

Processed images from summertime had a more limited value range. A typical example of a spectral similarity map for summer time is plotted in figure 12. Although the non-saline areas in the north and single, recently irrigated, wet fields had a spectral similarity of 0, the value range over the agricultural area (including irrigated and non-irrigated sites) was only from 0.5 to 1. Summer images do not show pronounced differences over the area of interest, and it is difficult to directly distinguish between saline and non-saline areas. One therefore can try to obtain uncalibrated salinity maps using alternative image transformations. The NDVI can be used as such an alternative image transformation because plant growth is reduced by soil salinity.

One drawback of the NDVI in the context of salinity mapping is the fact that different plants grow on different levels of salinity and therefore the index is an ambiguous indicator for the extent of salinity. Moreover, if the absence of vegetation or the reduced vigour is not due to the presence of salt, the NDVI predicts wrong results. The reduced vitality could likewise be related to the absence of essential nutrients. In wintertime, practically no vegetation is present and it is

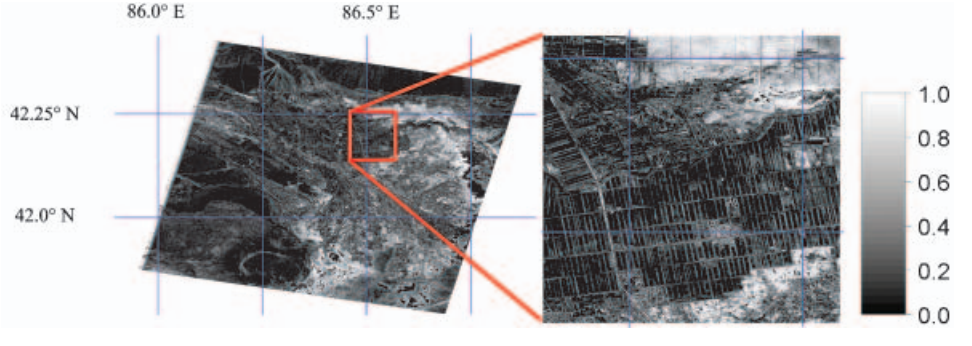

Figure 11. Map of spectral similarity calculated with the SCM (11 November 2002). White areas indicate a high spectral similarity to the reference spectrum.

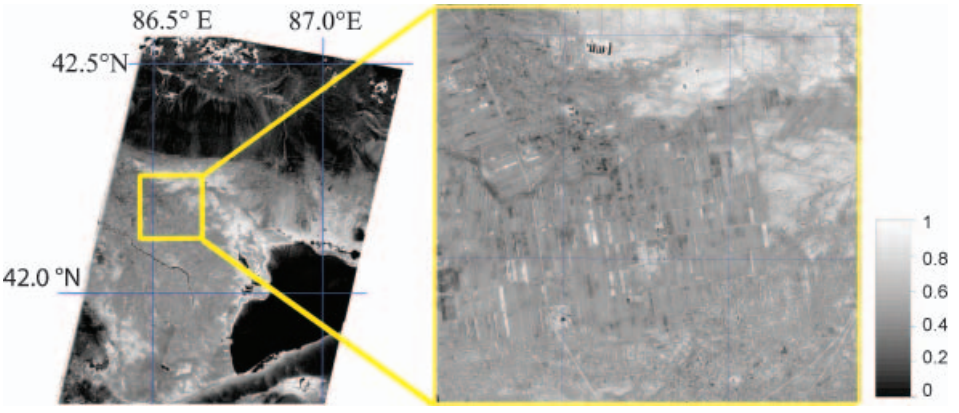

Figure 12. Uncalibrated salinity map calculated with the Spectral Correlation Mapper. The images (mosaic of two ASTER images) were recorded on 3 September 2003.

therefore not meaningful to use the NDVI instead of the Spectral Correlation Mapper.

Several completely saline areas are present in the Yanqi Basin and could potentially be used to obtain an image derived reference spectrum. For the image of 11 November 2002, two uncalibrated salinity maps were calculated based on two different image derived reference spectra. Although the reference spectra were not identical, the patterns of the uncalibrated salt maps were similar and therefore could be scaled to the same electrical conductivity values with slightly different relationships between field data and remote sensing data. A comparison between the two similarity maps calculated with a different reference spectra is shown in figure 13. The correlation coefficient is very high but the offset shows that the different reference spectra do not yield identical results. The lowest values are around 0.8. These low values are exclusively found in the northern part of the Basin.

4. Combining remote sensing and field data

Two types of uncalibrated salinity maps have been calculated: spectral similarity for all images and the NDVI for images obtained in summer. The next step is combining

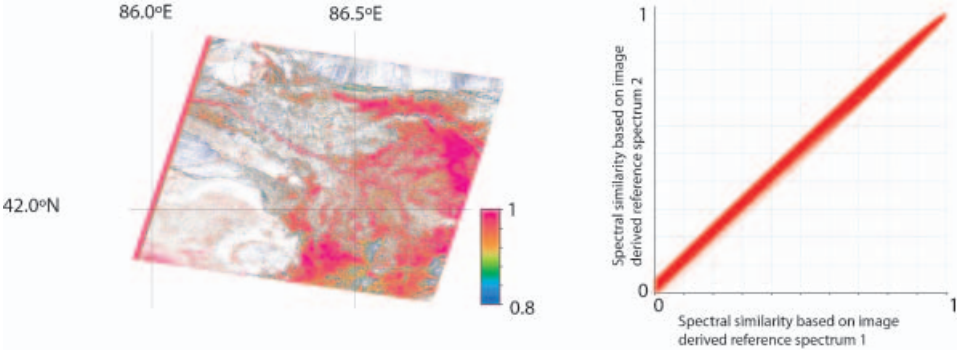

Figure 13. Ratio between two maps calculated with a different reference spectrum (see left) and their pixelwise comparison (see right). The image was recorded on 11 November 2002. The white areas have a spectral similarity of zero.

field data with the uncalibrated salinity maps. Field data are represented by the scaled EM38 measurements.

Before one can plot field data vs uncalibrated salinity maps, two important points have to be taken into account: the time gap between measurements on the ground and the date on which the image was obtained. Moreover, inaccuracies of the coordinates of ground measurement sites have to be taken into account.

4.1 *Comparing measurements on the ground with satellite images from a different dates*

It is very difficult to get satellite images of exactly the same date as field work, especially when field work is performed over a long time. Remote sensing data were not available for the dates field data were obtained. The image from 11 November 2002 is with 1 month delay closest in time to fieldwork. If the parameter of interest, in this case electrical conductivity of the soil, is subject to quick changes, it should only be compared with a satellite image of the same date. Fortunately, the Yanqi Basin features large areas where soil conductivity is not subject to quick changes. Measurements obtained at such locations can be compared with remotely sensed images even if the dates are not identical.

To identify these areas, it is helpful to recall the factors influencing the total amount as well as the distribution of salt in a soil column. The capillary rise of saline groundwater will increase the amount of salt. On the other hand, a major rain event or the irrigation of a field will remove the accumulated salts from the surface layer, changing within minutes the electrical conductivity profile of the soil as well as the surface properties recorded by the satellite. The annual precipitation of 20 mm is, however, by far insufficient to flush down the salt accumulated by the continuous evaporation through the soil column. If a field is not irrigated, only capillary rise will change the amount and distribution of salt in the soil column.

This process is slow. In the Yanqi Basin, salinization was triggered by irrigation. Over the non-irrigated areas, salt accumulated for at least 50 years. If $1.2\,\mathrm{m\,a^{-1}}$ groundwater (equal to the potential ET) would evaporate with a solute concentration of $2.1\,\mathrm{g\,l^{-1}}$ (equal to the highest concentration of salt found in drainage water), the annual increase of salt would be around $2.5\,\mathrm{kg\,m^{-2}\,a^{-1}}$. This value is unrealistically high as the soil column between groundwater and the atmosphere will reduce the potential ET significantly. Moreover, the concentration of salt in groundwater does not reach the high salt concentrations of the drainage water, but even if the increase in the total amount of salt was $2.5\,\mathrm{kg\,m^{-2}\,a^{-1}}$, it is still small compared with the total amount of salt at non-irrigated stations: station 16, an example of a moderately saline, non-irrigated station contains about $60\,\mathrm{kg\,m^{-2}}$ salt within the soil column from the surface down to the groundwater table at 1.8 m.

Besides variations of the total amount of salt, the water content influences the electrical conductivity in the field and even may change the spectral properties of the surface. In this approach, field data consist of an electrical conductivity measure independent of field conditions. The water content in the non-irrigated soil does not vary quickly, as the only source of water is groundwater. Still, the variation of the depth to groundwater could influence the spectral properties at the surface. Even though changes of the groundwater table up to 10 cm per irrigation cycle have been observed under irrigated fields, the annual changes of the groundwater table under non-irrigated sites are much smaller. That variations in the groundwater table significantly influence the spectral properties is therefore unlikely, but the potential

constraint is also addressed by deriving the reference spectrum used from the image processed.

4.2 *Inaccuracies of the location of measurement sites on the ground*

Coordinates of the centre of every EM38 site were obtained with a hand-held GPS. The accuracy of this hand-held GPS is around 10 m. On the assumption that the maximum error of position is no more than claimed by the manufacturer, the measurement layout could overlap with each of the eight surrounding pixels. Therefore the minimum and maximum of these pixels define the upper and lower limit of the real spectral similarity while the probable value is the area-weighted value around the measured location.

5. Results

5.1 *Combining field data with uncalibrated salinity maps*

For 51 locations, the average electrical conductivity over an area equal in size to the pixel has been quantified as described in §3.2. These electrical conductivity values represent the first 30 cm of the soil column. ASTER images are not large enough to cover the entire region, therefore not all measurement sites are covered by every image. Nevertheless, at least 13 and at most 26 stations were within in the images processed. For the reasons discussed in §4.1, only non-irrigated sites are admissible for comparison. The measurements over the non-irrigated sites have been obtained during the field campaign from September to October 2002, see §3.2. Table 2 gives an overview of the images processed, the number of non-irrigated sites included in the image and the method how uncalibrated salinity maps were calculated.

As described in §4.2, the positions of the EM38-layout centres were considered exact and the values at these locations were used to calculate a linear regression for every image processed. The minimum and maximum of the surrounding pixels, plotted as error bars (see figure 14), indicate the largest and smallest possible value of spectral similarity. The sometimes wide error bars reflect the situation found in the Yanqi Basin: homogeneous areas were present but their spatial extent was mostly small.

5.2 *Field data vs spectral similarity*

All images were processed with the SCM. Figure 14 plots for the uncalibrated salinity maps of 11 November 2002 and 28 March 2001 the relation between remote sensing and field data. Only electrical conductivities obtained at non-irrigated sites correlate with the corresponding values from the uncalibrated salinity maps. The

Table 2. Overview of processed images.

Date of the ASTER image processed	Number of non-irrigated measurement sites included in the image	Method used to calculate uncalibrated salinity maps
28 March 2001 (Winter)	20	SCM
12 August 2001 (Summer)	26	SCM, NDVI
13 November 2001 (Winter)	13	SCM
11 November 2002 (Winter)	24	SCM
3 September 2003 (Summer)	21	SCM, NDVI

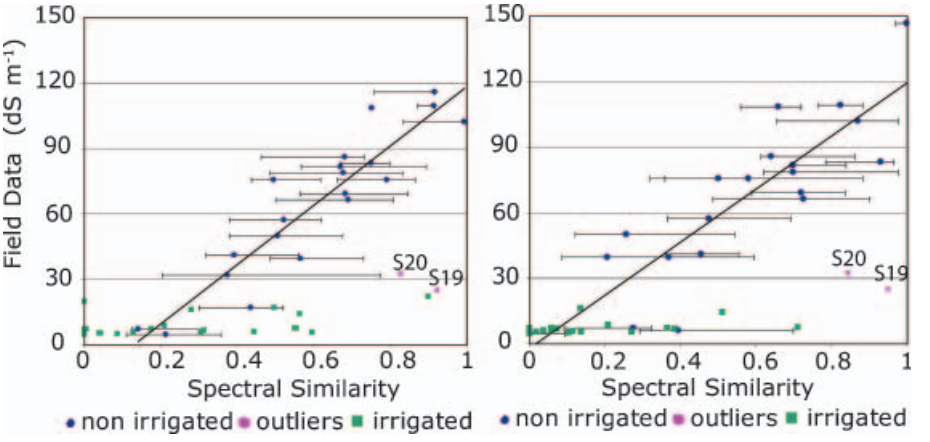

Figure 14. Field data (y-axis) versus pixel similarity (x-axis) for (see left) 11 November 2002 and (see right) 28 March 2001. Green points are from irrigated areas, blue points from non-irrigated sites.

found relations and corresponding correlation coefficients are listed in table 3. Two non-irrigated sites, S19 and S20, do not fit into the correlation. The two stations are situated close to each other, in the southeastern part of the Basin. The measured conductivities on the ground are far below the value expected from spectral similarity. Both outliers can be explained with the electrical conductivity profile found exclusively at these specific locations. Compared with all other non-irrigated sites, the electrical conductivity profiles at both stations clearly have a different shape. A typical electrical conductivity profile of a non-irrigated site is presented in figure 5: electrical conductivity gradually decreases with depth. At the outlier stations S19 and S20, high conductivities were measured in the first 10 cm of the profiles. Below this layer, electrical conductivity dropped to only 10% of the first 10 cm. At all other sites, such small values were observed at depths of at least 60 cm. The interpretation of EM38 data yields an average electrical conductivity of the first 30 cm. The uncalibrated salinity maps, which take into account the surface only, therefore overestimate electrical conductivity values. The shape of an electrical conductivity profile depends on the soil type. The clay content determines the relationship between depth and evaporation and therefore the distribution of salt in the soil column. If a soil map is available, different relations between field data and remotely sensed data can be developed for every soil type.

Besides stations S19 and S20, the image of 28 March 2001 has an additional outlier (not printed in the plot). This point fitted well into the correlations obtained for all other images. The reason why the surface composition was different on 28 March compared with all other dates cannot be explained with the available data.

Table 3. Linear relationships between uncalibrated salinity maps and field data.

	Function	R^2
28 March 2001	$y=121.4x-2.1$	0.74
3 September 2003 (NDVI)	$y=-357.9x+142.7$	0.61
11 November 2002	$y=135.5x-17.4$	0.85
12 August 2001 (NDVI)	$y=-272.0x+148.8$	0.63
13 November 2001	$y=228.7x-110.9$	0.75

Images recorded in winter time and processed with SCM showed the best correlation between spectral similarity and field data. However, the spectral flatness of the summer images did not allow us to distinguish satisfactorily between saline and non-saline pixels using the SCM.

5.3 *Field data vs. NDVI*

Compared with the SCM, the NDVI showed higher correlations between raster and field data for images obtained in summer. A comparison of the two methods for the same date (3 September 2003) is plotted in figure 15.

The left side of this figure plots the relation between field data and spectral similarity. Even non-saline pixels still have a spectral similarity of 0.4. The right-hand side of figure 15 plots the relation between field data and the NDVI. As expected, the smallest NDVI values are found around the most saline stations. Despite all implicit assumptions made by defining the NDVI as an uncalibrated salinity map (see §3.3.3), a correlation could be established, see table 3. Another comparison between SCM and NDVI for a summer image is presented in figure 16. The spectral similarity of the pixels is too high to distinguish between saline and

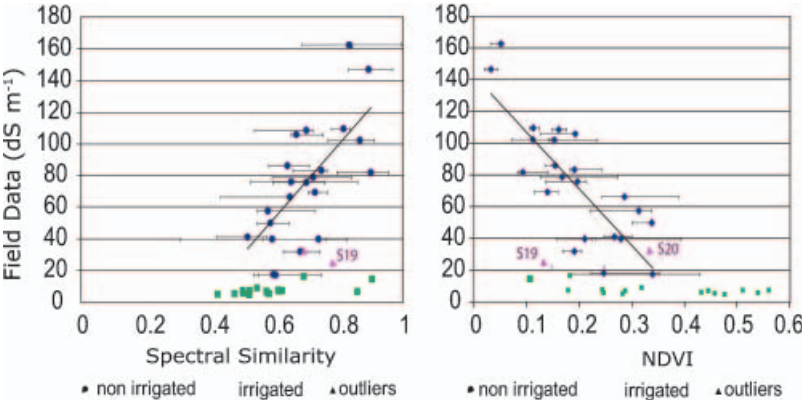

Figure 15. Field data versus spectral similarity and NDVI (3 September 2003).

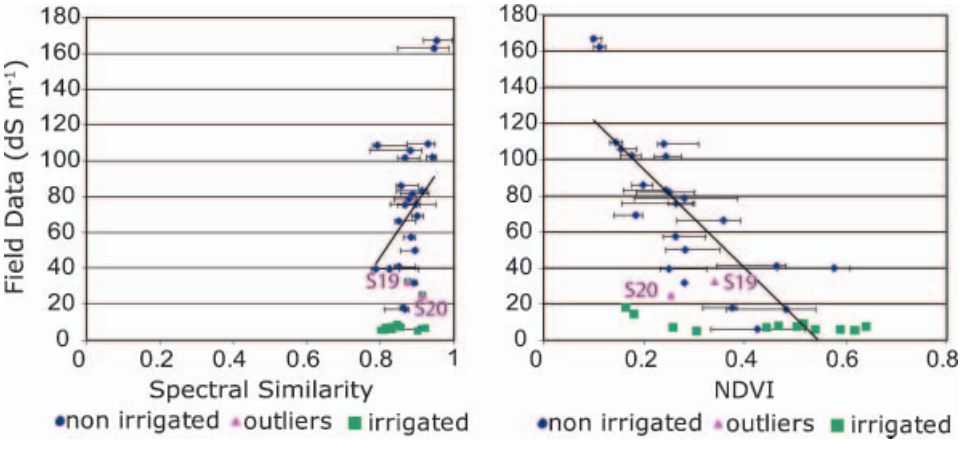

Figure 16. Field data vs. spectral similarity and NDVI (12 August 2001).

non-saline areas. However, a significant correlation between field data and the NDVI was found, see table 3.

5.4 *Summary of obtained relations between field data and uncalibrated salinity maps*

Compared with the NDVI–field data relations, correlation coefficients are remarkably higher if the uncalibrated salinity maps were obtained with the SCM. The highest correlation coefficients were found with the image obtained on 13 November. This image was closest in time to the measurements over the non-irrigated sites in September 2002.

6. Conclusions

The goal of this study was to map the electrical conductivity of the soil at a regional level. The correlations found between field data and raster data allowed five uncalibrated salinity maps obtained from SCM and NDVI transformations performed on ASTER imagery to be scaled to continuous electrical conductivity maps. The combination of methods on different scales was the key to the derivation of such maps. The combination of soil samples with the EM38 allowed large areas to be mapped within a reasonable time. Using saturated paste conductivities as a reference, the values obtained are independent of the field conditions. Even though quantifying salinity using the EM38 is quick, no continuous map can be produced over a large area. Only the combination with remotely sensed data allows a conductivity map to be produced over such a large area.

The accuracy of the electrical conductivity maps depends on the quality (and consistency) of field data, and on the extent to which the string of assumptions made to combine these two methods is fulfilled. In the case of the Yanqi Basin, the quality of field data does not limit the reliability of the method, as data are consistent between the different methods and the outliers could be explained. Very high correlation coefficients between saturated paste conductivities, interpreted EM38 measurements as well as inverted resistivity measurements soundings were found.

One assumption made when combining the two methods was that the electrical conductivity profiles at all stations are similar. The outlier stations 19 and 20 do not fulfil this condition. If the shape of the electrical conductivity profiles varies considerably, this method yields wrong results. If there is a large variation of soil types within the area of interest, field data should be obtained on every soil type separately.

The best agreement between the uncalibrated salinity maps and the measurements on the ground was found for the image that was acquired closest to the period of field data. Soil salinization is a slow process but soil electrical conductivity increases continuously. This increase is not distributed evenly over the area of consideration: a different depth to groundwater is related to a different evaporation rate and to a different salinization rate. It is therefore expected that the correlation coefficient decreases with an increasing temporal gap between the image acquisition date and the period of field data. The correlation coefficients for different dates seem to support this hypothesis.

This method can be applied to other regions, provided the same assumptions are fulfilled. The presence of sufficiently large and well distributed, non-irrigated areas (preferably several times the extent of a pixel) is required. This is often the case, as areas between fields are usually large enough to fulfil this constraint.

Acknowledgments

We thank the Department of Water Resources in Korla, the People's Security Bureau in Yanqi city as well as Professor Dong from Xinjiang Agricultural University, Urumqi. Only with their kind support was fieldwork possible in this area. We further thank the Institute of Geophysics, ETH Zurich for providing some of the equipment used. Finally, we gratefully acknowledge the valuable suggestions made to us by the anonymous reviewers.

References

Ben-Dor, E., Patkin, K., Banin, A. and Karnieli, A., 2002, Mapping of several soil properties using DAIS-7915 hyperspectral scanner data—a case study over clayey soils in Israel. *International Journal of Remote Sensing*, **23**, pp. 1043–1062.

Csillag, F., Pasztor, L. and Biehl, L.L., 1993, Spectral band selection for the characterization of salinity status of soils. *Remote Sensing of Environment*, **43**, pp. 231–242.

de Carvalho O. and Meneses, P.R., 2000, Spectral correlation mapper—an improvement on the spectral angle mapper (SAM). In *9th Airborne Earth Science Workshop*, Vol. 00–18. Jet Propulsion Laboratory.

Dong, X., Jiang, T. and Jiang, H., 2001, Study on the pattern of water resources utilisation and environmental conservation of Yanqi Basin. In *Development, Planning and Management of Surface and Groundwater Resources. Vol. A of IAHR Congress Proceedings*, G. Li (Ed.), pp. 333–340 (Beijing: Tsinghua University Press).

Dwivedi, R.S. and Rao, B.R.M., 1992, The selection of the best possible Landsat TM band combination for delineating salt-affected soils. *International Journal of Remote Sensing*, **13**, pp. 2051–2058.

Geonics Limited 2001, EM38-ground conductivity meter operating manual. Technical report.

Halvorson, A.D. and Rhoades, J.D., 1976, Field mapping soil conductivity to delineate dryland saline seeps with 4-electrode technique. *Soil Science Society of America Journal*, **40**, pp. 571–575.

Hendrickx, J.M.H., Borchers, B., Corwin, D.L., Lesch, S.M., Hilgendorf, A.C. and Schlue, J., 2002, Inversion of soil conductivity profiles from electromagnetic induction measurements: theory and experimental verification. *Soil Science Society of America Journal*, **66**, pp. 673–685.

Hillel, D., 1990, *Out of the Earth: Civilization and the Life of the Soil* (New York: Free Press).

Hillel, D., 2000, *Salinity Management for Sustainable Irrigation: Integrating Science, Environment and Economics* (Washington, DC: World Bank).

Howari, F.M., 2003a, A comparison of spectral matching algorithms for identifying natural salt crusts. *Journal of Applied Spectroscopy*, **70**, pp. 782–787.

Howari, F.M., 2003b, The use of remote sensing data to extract information from agricultural land with emphasis on soil salinity. *Australian Journal of Soil Research*, **41**, pp. 1243–1253.

Howari, F.M., Goodell, P.C. and Miyamoto, S., 2002, Spectral properties of salt crusts formed on saline soils. *Journal of Environmental Quality*, **31**, pp. 1453–1461.

Jakeman, A.J., Nix, H.A. and Ghassemi, F., 1995, *Salinisation of Land and Water Resources: Extent, Management and Human Causes* (Wallingford: CAB International).

Kalra, N.K. and Joshi, D.C., 1996, Potentiality of Landsat, SPOT and IRS satellite imagery for recognition of salt affected soils in Indian arid zone. *International Journal of Remote Sensing*, **17**, pp. 3001–3014.

Lowrie, W., 1997, *Fundamentals of Geophysics* (Cambridge: Cambridge University Press).

McKenzie, R., George, R., Woods, S., Cannon, M. and Bennett, D., 1997, Use of the electromagnetic-induction meter (EM38) as a tool in managing salinisation. *Hydrogeology Journal*, **5**, pp. 37–50.

McNeil, J., 1980, Electromagnetic terrain conductivity measurement at low induction numbers. Geonics Technical Note TN6. Technical report.

McNeill, J., 1992, Rapid, accurate mapping of soil salinity by electromagnetic ground conductivity meters. In *Advances in Measurement of Soil Physical Properties: Bringing Theory into Practice*, G.C. Topp, R.J. Luxmoore, S.H. Mickelson and N.H. Rhodehamel (Eds) (Madison, WI: Soil Science Society of America).

Metternicht, G. and Zinck, J.A., 1997, Spatial discrimination of salt-and sodium-affected soil surfaces. *International Journal of Remote Sensing*, **18**, pp. 2571–2586.

Metternicht, G.I. and Zinck, J.A., 2003, Remote sensing of soil salinity: potentials and constraints. *Remote Sensing of Environment*, **85**, pp. 1–20.

Mulders, M.A., 1987, *Remote Sensing in Soil Science* (Amsterdam: Elsevier).

Oldeman, L.R., Hakkeling, R.T.A. and Sombroek, W.G., 1991, *World Map of the Status of Human-induced Soil Degradation: an Explanatory Note*, 2nd edn (Wageningen: International Soil Reference and Information Centre).

Rao, B.R.M., Sankar, T.R., Dwivedi, R.S., Thammappa, S.S., Venkataratnam, L., Sharma, R.C. and Das, S.N., 1995, Spectral behavior of salt-affected soils. *International Journal of Remote Sensing*, **16**, pp. 2125–2136.

Rhoades, J., 1996, Salinity: electrical conductivity and total dissolved solids. In *Methods of Soil Analysis: Part 3—Chemical Methods*, Soil Science Society of America Book Series Number 5, pp. 417–435 (Madison, WI: Soil Science Society of America).

Rhoades, J.D., Kandiah, A. and Mashali, A.M., 1992, *The Use of Saline Waters for Crop Production* (Rome: Food and Agriculture Organization of the United Nations).

Rhoades, J.D., Lesch, S.M. and Chanduvi, F., 1999, Soil salinity assessment: methods and Interpretation. FAO Irrigation and Drainage Paper 57. FAO, Rome.

Rhoades, R. and Miyamoto, S., 1990, Testing soils for salinity and sodicity. In *Soil Testing and Plant Analysis*, 3rd edn, R.L. Westerman (Eds), pp. 299–336 (Madison, WI: Soil Science Society of America).

Richards, L., 1954, *Diagnosis and Improvement of Saline and Alkali Soils*, Agriculture Handbook No. 60 (Washington DC: US-Salinity Laboratory, US Department of Agriculture).

Singh, R.P., Kumar, V. and Srivastav, S.K., 1990, Use of microwave remote-sensing in salinity estimation. *International Journal of Remote Sensing*, **11**, pp. 321–330.

Taylor, G.D.R., 2000, Salinity mapping with hyperspectral imagery. Available at: www.bees.unsw.edu.au/research/remotesensing/salinity1.html (accessed September 2001).

Taylor, G.R., Mah, A.H., Kruse, F.A., Young, K.S., Hewson, R.D. and Bennett, B.A., 1996, Characterization of saline soils using airborne radar imagery. *Remote Sensing of Environment*, **57**, pp. 127–142.

Telford, W.M., Geldart, L.P. and Sheriff, R.E., 1990, *Applied Geophysics*, 2nd edn (Cambridge: Cambridge University Press).

Thome, K., 1999, Algorithm theoretical basis document for ASTER Level2B1 surface radiance and ASTER Level2B5 reflectance. University of Arizona, Tucson, AZ, p. 28.

Wiegand, C.L., Rhoades, J.D., Escobar, D.E. and Everitt, J.H., 1994, Photographic and videographic observations for determining and mapping the response of cotton to soil-salinity. *Remote Sensing of Environment*, **49**, pp. 212–223.

Yuhas, R., Goetz, A. and Boardman, J., 1992, Discriminating among semi-arid landscape endmembers using spectral angle mapper (SAM) algorithm. In *Third Annual JPL Airborne Geoscience Workshop*, Vol. 92–14, 1, pp. 147–149 (Jet Propulsion Laboratory).